

Heralded single-photon partial coherence

P. Ben Dixon,¹ Gregory Howland,¹ Mehul Malik,² David J. Starling,¹ R. W. Boyd,^{1,2} and John C. Howell¹

¹*Department of Physics and Astronomy, University of Rochester, Rochester, New York 14627, USA*

²*Institute of Optics, University of Rochester, Rochester, New York 14627, USA*

(Received 12 January 2010; published 2 August 2010)

We study transverse spatial coherence of approximately localized single-photon states. We demonstrate nonlocal control over single-photon spatial coherence via projective measurements of an entangled twin and provide a theoretical interpretation from quantum coherence theory. Our results show that the spatial coherence of a single-photon state behaves similarly to that of a classical optical field, although the coincidence measurement adds a degree of freedom.

DOI: [10.1103/PhysRevA.82.023801](https://doi.org/10.1103/PhysRevA.82.023801)

PACS number(s): 42.50.Ar, 42.65.Lm, 03.67.Dd, 42.50.Dv

I. INTRODUCTION

Optical spatial coherence, characterizing correlations between optical fields at distinct points, plays a key role in the understanding of classical and quantum phenomena. While coherence in general has been studied since at least the times of Thomas Young and Émile Verdet in the 19th century, spatial coherence for classical optical fields was only put on firm theoretical footing in the early 20th century by Zernike and van Cittert [1,2], followed closely by experimental work [3].

Technological advances in recent decades, such as powerful lasers and fast, efficient photon counters, have enabled the study of nonclassical (quantum) optical fields. Spontaneous parametric down-conversion (SPDC) in a nonlinear optical crystal allows for the creation of entangled photons as well as approximately localized single-photon states through heralding [4]. The spatial properties of such states have been extensively described in terms of position-momentum entanglement [5,6], ghost imaging [7], and ghost diffraction [8]. Related research includes the creation of entangled images—investigated both theoretically and experimentally [9–11]—sub-Rayleigh diffraction interference [12], Gaussian state imaging [13], and high-dimensional quantum key distribution [14]. Because the transverse spatial domain consists of an infinite number of orthogonal modes, it possesses tremendous data capacity for key distribution or other data transmission schemes even at the single-photon level [15,16]. Theoretical and experimental treatments typically assume complete single-photon spatial coherence—namely, that each individual photon perfectly interferes with itself spatially.

Although previous work has focused on establishing a Zernike–van Cittert–type relation for down-converted fields, questions about what was ultimately observable and how to characterize observations remained. We extend this work to describe two-point partial coherence for a single photon, rather than a down-converted biphoton. We provide a theoretical model from quantum coherence theory and experimental observations inspired by Thompson and Wolf [3]. In particular, we clarify the role of quantum birth zones in SPDC sources and observe the zero crossing of the field’s partial coherence. Birth zones are the quantum analog of independent classical emitters; they characterize the heralded single photon’s coherence properties.

II. THEORY

We consider the following scheme (the experimental setup is shown in Fig. 1): a laser beam pumps an SPDC crystal and we approximate the output as an entangled two photon state [17]:

$$|\psi\rangle \propto \int dx_s dx_i \exp\left(-\frac{x_s + x_i}{\Delta_p}\right)^2 \times \exp\left(-\frac{x_s - x_i}{\Delta_c}\right)^2 a^\dagger(x_s)a^\dagger(x_i)|0\rangle, \quad (1)$$

where Δ_p is the $1/e^2$ beam radius (in intensity) at the SPDC crystal, and Δ_c is the $1/e^2$ transverse correlation radius, or birth zone radius, at the crystal. A beamsplitter separates this output state into signal and idler beams (denoted by s and i , respectively).

We use the idler beam to herald a photon in the signal beam. The idler beam passes through optics creating a scaled image of the crystal face where an adjustable-width slit is placed, followed by a bucket detector. We detect at the image plane to eliminate the propagation effects of the idler photon. The transverse field operator at this image plane is identical to the operator at the crystal output face,

$$\hat{E}_i^{(-)}(x_i) \propto a^\dagger(M_i x_i), \quad (2)$$

where x_i and is the transverse position variable of the idler beam at this plane, and M_i is the scaling term. Closing the adjustable idler slit in this arm controls the number of transverse SPDC birth zones contributing to a coincident detection.

We propagate the signal beam and are interested in the two-point degree of coherence of this propagated signal beam. The transverse field operator after the collimating lens is the transverse operator at the crystal output face integrated over the propagation kernel (the first exponential can be discarded if the field propagates to the far field),

$$\hat{E}_s^{(-)}(x_s) \propto \int dx_1 a^\dagger(x_1) \exp\left(i\frac{k}{z}x_1^2\right) \times \exp\left(-i\frac{k}{z}(M_s x_s)x_1\right), \quad (3)$$

where k is the wave number of the light, x is the transverse position, z is the propagation distance, and M_s is a scaling

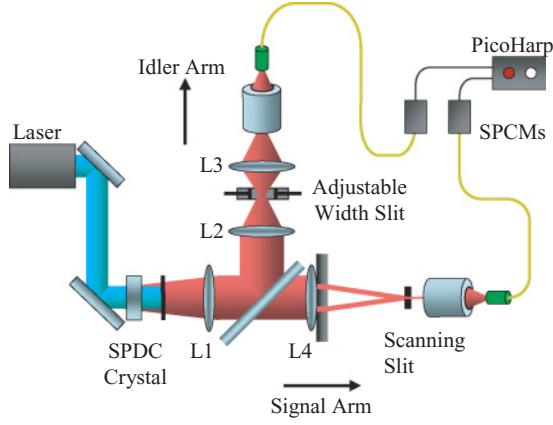


FIG. 1. (Color online) A 325 nm collimated pump undergoes Type-I nondegenerate collinear SPDC at a nonlinear crystal. The crystal face is imaged onto an adjustable-width slit in the idler arm and a computer controlled scanning 50 μm slit in the signal arm. The diffraction pattern from the double slit mask in the signal arm is profiled by the scanning slit. Photons are detected with single-photon counting modules. A PicoHarp coincidence circuit correlates these measurements and provides results to data logging software.

term for the signal beam. Subscript 1 indicates the variable is for the plane of the crystal face.

In general, for nonheralded photons, the two point degree of coherence for a given state and field operators is

$$g^{(1)}(x_a, x_b) = \frac{\langle \psi | \hat{E}^{(+)}(x_a) \hat{E}^{(-)}(x_b) | \psi \rangle}{\sqrt{\langle \psi | \hat{E}^{(+)}(x_a) \hat{E}^{(-)}(x_a) | \psi \rangle \times \langle \psi | \hat{E}^{(+)}(x_b) \hat{E}^{(-)}(x_b) | \psi \rangle}}. \quad (4)$$

The effect of heralding a signal photon with an idler photon, as in our case, is to make the following substitution:

$$\langle \psi | \hat{E}_s^{(+)}(x_a) \hat{E}_s^{(-)}(x_b) | \psi \rangle \rightarrow \int_{\text{slit}} \langle \psi | \hat{E}_s^{(+)}(x_a) \hat{E}_i^{(+)}(x_i) \hat{E}_i^{(-)}(x_i) \hat{E}_s^{(-)}(x_b) | \psi \rangle dx_i. \quad (5)$$

The heralding introduces the variable x_i which is integrated out, however the limits of spatial integration can be controlled, thus adding a degree of freedom.

We make the substitution and consider the case of symmetric points ($x_b = -x_a$) and use a slit width of W . The numerator becomes

$$\frac{\exp\left(\frac{-(4AC+D^2)x^2}{4C}\right) \times \left[\text{Erf}\left(\frac{CW+iDx}{2\sqrt{C}}\right) + \text{Erf}\left(\frac{CW-iDx}{2\sqrt{C}}\right) \right]}{\sqrt{\frac{4C}{\pi F^2} [(N^2+1)^2 + F^2]}} \quad (6)$$

and the denominator becomes

$$\frac{\exp\left(\frac{-(4AC+B^2)x^2}{4C}\right) \times \left[\text{Erf}\left(\frac{CW+Bx}{2\sqrt{C}}\right) + \text{Erf}\left(\frac{CW-Bx}{2\sqrt{C}}\right) \right]}{\sqrt{\frac{4C}{\pi F^2} [(N^2+1)^2 + F^2]}}. \quad (7)$$

The single photon $g^{(1)}$ is then the quotient of these:

$$g^{(1)}(x, -x; W) = \exp\left(\frac{-(B^2 + D^2)x^2}{4C}\right) \times \left[\frac{\text{Erf}\left(\frac{CW+iDx}{2\sqrt{C}}\right) + \text{Erf}\left(\frac{CW-iDx}{2\sqrt{C}}\right)}{\text{Erf}\left(\frac{CW+Bx}{2\sqrt{C}}\right) + \text{Erf}\left(\frac{CW-Bx}{2\sqrt{C}}\right)} \right]. \quad (8)$$

The terms used above are defined as follows:

$$A = \frac{2F^2 M_s^2 (N^2 + 1)}{\Delta_p^2 [(N^2 + 1)^2 + F^2]}, \quad (9)$$

$$B = \frac{-4F^2 M_i M_s (N^2 - 1)}{\Delta_p^2 [(N^2 + 1)^2 + F^2]}, \quad (10)$$

$$C = \frac{2M_i^2 (N^2 + 1) (F^2 + 4N^2)}{\Delta_p^2 [(N^2 + 1)^2 + F^2]}, \quad (11)$$

$$D = \frac{-4F M_i M_s (N^4 - 1)}{\Delta_p^2 [(N^2 + 1)^2 + F^2]}, \quad (12)$$

where $N = \Delta_p / \Delta_c$ is the number of birth zones excited by the pump, this quantity is identical to the R parameter used by Fedorov *et al.* for quantifying entanglement [18], and $F = \Delta_p^2 k / 2z$ is the Fresnel number, a geometric factor related to the propagation of the pump beam. As the field propagates to the far field, this Fresnel number goes to zero; the formula for the far field then is the first order expansion in F . Although the error function arguments in Eq. (8) are complex, the sum of the error functions themselves is purely real due to symmetric points being used.

The nonheralded two-point degree of coherence $g_{nh}^{(1)}$ at this plane uses the SPDC state with the idler photon traced out over all space, effectively extending the idler slit width to infinity. The resulting symmetric two-point coherence is

$$g_{nh}^{(1)}(x, -x) = \exp\left(\frac{-(B^2 + C^2)x^2}{4A}\right). \quad (13)$$

Figure 2 shows representative $g^{(1)}(x, -x; W)$ curves as a function of W for several values of N . The parameters for A, B, C, D , and x correspond to those used in the experiment. As $N \rightarrow 1$ the degree of coherence for the heralded signal photon is less and less affected by the opening of the idler slit. This mirrors the classical behavior of unity degree of coherence for a single emitter field, regardless of emitter size. For $N \gg 1$ the photon's partial coherence exhibits oscillatory behavior similar to the classical behavior described by the Zernike-van Cittert theorem which assumes infinitesimally small emitters. One can see that when N is sufficiently large, we expect the degree of coherence to exhibit a phase inversion for certain slit widths, represented in Fig. 2 by the curves dipping below zero. This would manifest itself in an interference pattern as peaks becoming troughs and vice versa. The corresponding nonheralded degree of coherence for these representative curves is less than 10^{-70} , essentially zero.

It is only near the image plane of the crystal that we can effectively post-select birth zones. By moving the idler slit toward the far field pattern of the crystal, either by moving the slit, or simply removing the idler arm focusing lens (lens L2

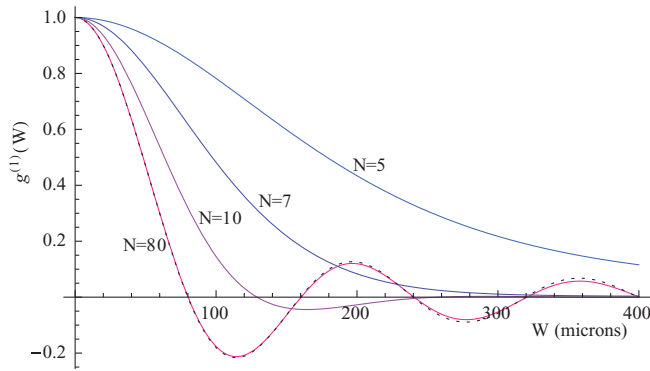


FIG. 2. (Color online) Representative theoretical predictions for heralded single-photon two-point degree of coherence from Eq. (8) for several numbers of birth zones excited by the pump as a function of idler slit width W . The only difference between the curves is the birth zone size. Relevant parameters for Eq. (8) are $A = 0.22 \text{ mm}^{-2}$, $B = 1.2 \text{ mm}^{-2}$, $C = 9.6 \text{ mm}^{-2}$, $D = -110 \text{ mm}^{-2}$, and $x = 743 \text{ }\mu\text{m}$. The dotted line is the behavior of a classical incoherent source with the intensity profile of the pump beam, apertured by the slit.

in Fig. 1) the birth zones would blend together incoherently due to diffraction. This would result in an effective birth-zone number less than N and $g^{(1)}$ in this type of setup could exhibit less or no oscillatory behavior. It should be noted that, just as in the classical Zernike–van Cittert theorem, accounting for finite bandwidth (as opposed to the single optical frequency theory provided here) results an average of weighted $g^{(1)}$ curves, each with a slightly different oscillation frequency. The predicted phase inversion and zero crossing would still be present however.

The expected coherence properties of heralded single photons have classical analogs, only in this case there is the added degree of freedom coming from the entangled twin photon used for heralding. This degree of freedom can be used to induce single-photon coherence inside spatially incoherent beams.

III. EXPERIMENT

The experimental apparatus is depicted in Fig. 1. Collimated light from an 8 mW, 325 nm HeCd laser, referred to as the pump, with a $1/e^2$ full width of approximately $1600 \text{ }\mu\text{m}$ was incident on a spectrally filtering dispersing prism. The pump was then incident on a 0.5 mm thick BiBO nonlinear optical crystal oriented for nondegenerate Type-I collinear SPDC. The resulting signal and idler photon bandwidths were centered on 633 nm and 667 nm, respectively. For these parameters the pump excites around 100 transverse birth zones of an approximate width $20 \text{ }\mu\text{m}$.

After the crystal, residual pump light was removed by a 325 nm stop-band notch filter. A dichroic mirror centered on 650 nm separated signal and idler photons into distinct optical paths.

For the signal arm, lens L1 (200 mm focal length, located 215 mm from the crystal face) very nearly collimates the down-conversion beam. Lens L4 (300 mm focal length, located 865 mm from lens L1) focuses the beam after it has passed through a double slit mask. A $50 \text{ }\mu\text{m}$ slit mounted on a

computer-controlled translation stage was placed at this focus (the image plane of the crystal). Scanning the stage in $5 \text{ }\mu\text{m}$ increments yielded the transverse interference profile of the signal beam. Observing the fringe visibility constitutes our measurement of the two-point degree of coherence between the two slits in the double slit mask. Ideally this fringe visibility is identical to the degree of coherence between the slits. These slits were $390 \text{ }\mu\text{m}$ wide and separated by $1490 \text{ }\mu\text{m}$ (center to center).

In the idler photon arm, lenses L1 (200 mm focal length and located 215 mm from the crystal) and L2 (250 mm focal length, located about 400 mm from lens L1) imaged the crystal face onto an adjustable-width slit with. After this slit, lens L3 (250 mm focal length) aided in photon collection. We note that the idler slit was scanned along the beam propagation axis such that it was in the ghost image plane of the signal arm detector. This ensures that we detect a sharp slit in coincidence however it effectively transfers all optical element placing error into the location of the idler slit. Slit misplacement would cause an effective slit width that is smaller than the true width.

Finally, the signal and idler beams were focused by $10\times$ microscope objectives onto multimode optical fibers connected to single-photon counting modules (SPCMs). The SPCMs were run in geiger mode to detect single photons and their output signals were sent to a PicoHarp counting unit which counted single-photon rates as well as the coincident rate. Counts were integrated for 20 s at each position of the scanning signal arm slit. The coincidence window was 3 ns. Data were recorded by a PC running LabView software. The detected patterns were thus built up from an ensemble of single photons, but the coherence properties were nevertheless a property of each photon individually.

IV. DATA

The theoretical and measured two-point coherence as a function of idler slit width is shown in Fig. 3. The dashed line shows the expected single photon $g^{(1)}$ from Eq. (8) with no variable slit placement error. The solid curve shows the expected theoretical $g^{(1)}$ with a effective slit scaling of $1/2$, corresponding to an error of location of about half an inch. Measured $g^{(1)}$ values are shown as points. These values were

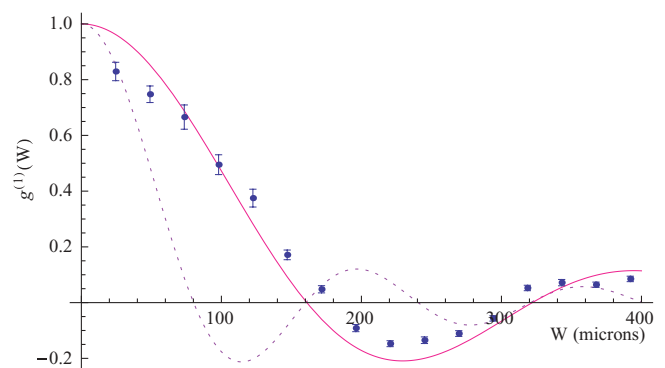


FIG. 3. (Color online) Measured two-point degree of coherence for the heralded photon are shown. The $g^{(1)}(W)$ from Eq. (8) is shown as a dotted line. The expected $g^{(1)}(W)$ with effective idler arm scaling is shown as a solid line.

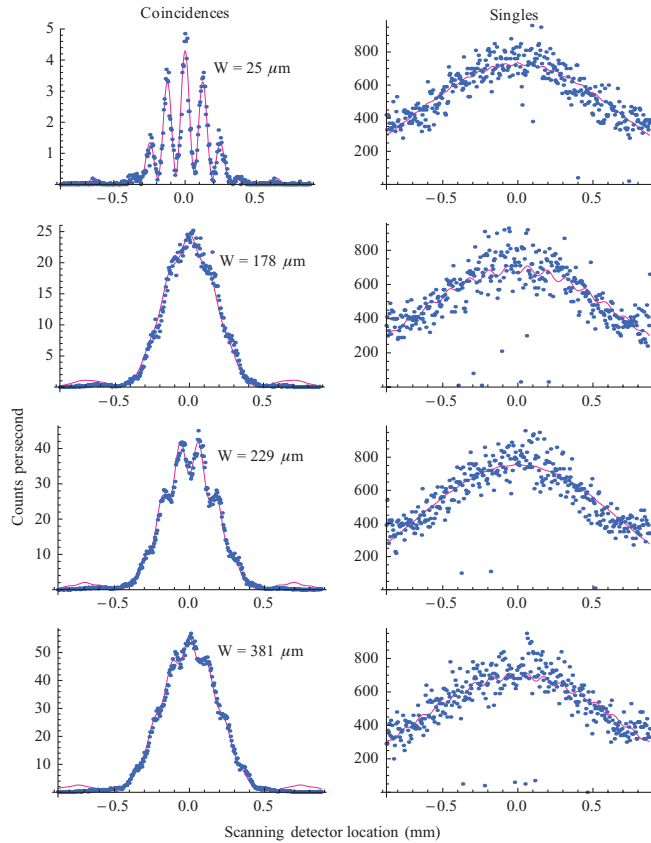


FIG. 4. (Color online) Detected interference patterns showing characteristics of interest for both heralded single photons (coincidences) and nonheralded photons (singles). Points are experimental data while lines are fits to the data.

found using a nonlinear least squares optimization to fit the detected interference pattern to the form of the expected pattern. Error bars represent 95% confidence intervals from the asymptotic standard errors of the optimization, and include random error only. The measured $g^{(1)}$ follows the expected behavior very well with one notable deviation: the measured

$g^{(1)}$ reaches a maximum that is less than unity for small idler slit widths. This is most likely due to the scanning slit having spatial extent and thus not being a true point detector. The measured $g_{nh}^{(1)}(W)$ values were distributed around zero, all had magnitude less than 0.05 and had error values of the same magnitude.

Representative interference scans used to determine $g^{(1)}$ and $g_{nh}^{(1)}$ are shown in Fig. 4. The points show experimental count data; the solid curves show theoretical expectation with best-fits. For nonheralded measurements we see no discernible coherence. The heralded single-photon case with controllable coherence achieves levels near unity. The interference pattern phase inversion for single photons is clearly visible.

V. CONCLUSION

We have measured the partial two-point transverse coherence ($g^{(1)}$) of heralded single-photon states. We projected entangled photon pairs into approximately localized single-photon states by detecting one of the photons and measuring the corresponding coincident photon. To characterize the single heralded photon, we eliminate the propagation effects of the heralding photon by detecting it at the image plane of the source. We were able to nonlocally control the remaining photon's partial transverse coherence with a slit in front of this image plane detector. The results show the behavior of such states to be well described by quantum coherence theory. Our discussion clearly describes quantum birth zones as a property of the single-photon source and shows how this source property governs the observed coherence. We have experimentally observed the predicted zero crossing of the degree of coherence and negative coherence.

ACKNOWLEDGMENTS

We thank Emil Wolf for discussions. This work was supported by the US Army Research Office through a MURI grant, and a Department of Defense PECASE award.

-
- [1] F. Zernike, *Physica* **5**, 785 (1938).
 - [2] P. H. van Cittert, *Physica* **1**, 201 (1934).
 - [3] B. J. Thompson and E. Wolf, *J. Opt. Soc. Am.* **47**, 895 (1957).
 - [4] C. K. Hong and L. Mandel, *Phys. Rev. Lett.* **56**, 58 (1986).
 - [5] P. H. S. Ribeiro, S. Pádua, J. C. Machado da Silva, and G. A. Barbosa, *Phys. Rev. A* **49**, 4176 (1994).
 - [6] P. H. Souto Ribeiro and G. A. Barbosa, *Phys. Rev. A* **54**, 3489 (1996).
 - [7] G. A. Barbosa, *Phys. Rev. A* **54**, 4473 (1996).
 - [8] D. V. Strekalov, A. V. Sergienko, D. N. Klyshko, and Y. H. Shih, *Phys. Rev. Lett.* **74**, 3600 (1995).
 - [9] A. Gatti, E. Brambilla, L. A. Lugiato, and M. I. Kolobov, *Phys. Rev. Lett.* **83**, 1763 (1999).
 - [10] M. N. O'Sullivan Hale, I. A. Khan, R. W. Boyd, and J. C. Howell, *Phys. Rev. Lett.* **94**, 220501 (2005).
 - [11] V. Boyer, A. M. Marino, R. C. Pooser, and P. D. Lett, *Science* **321**, 544 (2008).
 - [12] A. N. Boto, P. Kok, D. S. Abrams, S. L. Braunstein, C. P. Williams, and J. P. Dowling, *Phys. Rev. Lett.* **85**, 2733 (2000).
 - [13] B. I. Erkmen and J. H. Shapiro, *Phys. Rev. A* **77**, 043809 (2008).
 - [14] S. P. Walborn, D. S. Lemelle, M. P. Almeida, and P. H. Souto Ribeiro, *Phys. Rev. Lett.* **96**, 090501 (2006).
 - [15] R. M. Camacho, C. J. Broadbent, I. Ali-Khan, and J. C. Howell, *Phys. Rev. Lett.* **98**, 043902 (2007).
 - [16] C. J. Broadbent, P. Zerom, H. Shin, J. C. Howell, and R. W. Boyd, *Phys. Rev. A* **79**, 033802 (2009).
 - [17] C. K. Law and J. H. Eberly, *Phys. Rev. Lett.* **92**, 127903 (2004).
 - [18] M. V. Fedorov, M. A. Efremov, A. E. Kazakov, K. W. Chan, C. K. Law, and J. H. Eberly, *Phys. Rev. A* **69**, 052117 (2004).